Particle Accelerators
1984 Vol. 16 pp. 81–111
0031-2460/84/1602–0081$30.00/0

THE HEXATRON, A SIX-SIDED 4-GeV 300-μA CW MICROTRON

E. P. COLTON, E. A. CROSBIE. M. FOSS, H. E. JACKSON, K. W. JOHNSON, T. K. KHOE, M. J. KNOTT, R. L. KUSTOM, R. J. LARI, G. S. MAVROGENES, D. G. McGHEE, J. H. NOREM, J. MOENICH, W. F. PRAEG, H. TAKEDA, K. M. THOMPSON, and R. B. WEHRLE

Argonne National Laboratory, Argonne, IL 60439

(*Received December 19, 1983*)

The use of microtron accelerators to provide intense CW beams of electrons with energies in the 1–5 GeV range is discussed. Principles of operation are reviewed and a design is presented for a six-sided hexagonal microtron, a Hexatron, which is capable of furnishing 300 μA of electrons in 3 extracted beams whose energies can be varied individually from injection energy (185 MeV) to 4.0 GeV. Results of prototype studies of the hexatron sector magnets are discussed. Two configurations of beam optics, one with and one without shaping of the sector magnet edges, are shown to provide good beam containment. Calculations of effects of fluctuations in synchrotron radiation indicate that excellent beam emittance can be expected to full design energy. Methods for providing requisite alignment of optical elements and extraction of multiple beams are presented. Options for operating the Hexatron at energies above 4 GeV are also discussed.

I. INTRODUCTION

The generation of high-intensity electron beams at high energy (1–10 GeV) with high duty factor remains a serious challenge to accelerator technology. Several options have been explored recently for circumventing the low duty factor that characterizes the performance of conventional pulsed linear accelerators. These include use of an electron storage ring as a beam stretcher, continuous multi-turn recirculation through a conventional linac operated at reduced gradient, and CW acceleration in a microtron configuration. The power of the microtron concept derives from the ease of beam extraction and the possibility of simultaneous operation of several extracted beams at different intensities and energies. In this paper, we present the details of the design of a hexagonal microtron capable of furnishing 300 μA of electrons in 3 external beams whose energies can be varied individually from injection energy to 4.0 GeV in CW operation. In terms of current, number of beams, and energy variability, this is the most advanced conceptual design for a GeV CW system which has been discussed to date.

The hexagonal microtron (Hexatron) discussed here is one of a generic class of accelerators of relativistic particles in which the beam is recirculated through the same rf accelerating sections a finite number of times, usually in the range of 10–100. Compared with conventional linear accelerators, only moderate rf power is required because of the use of beam recirculation. The basic principle of operation is embodied in the microtron coherence condition which requires that the orbit geometry be adjusted to insure that the transit time from exit from the rf acceleration section to entrance on the next traversal of an rf section be an integral multiple of the rf period, thereby insuring uniform acceleration up to the extraction energy. In the approximation that the electron velocity, $v/c = 1$, this corresponds to the usual microtron condition that successive orbits increase in length by an integral number of rf

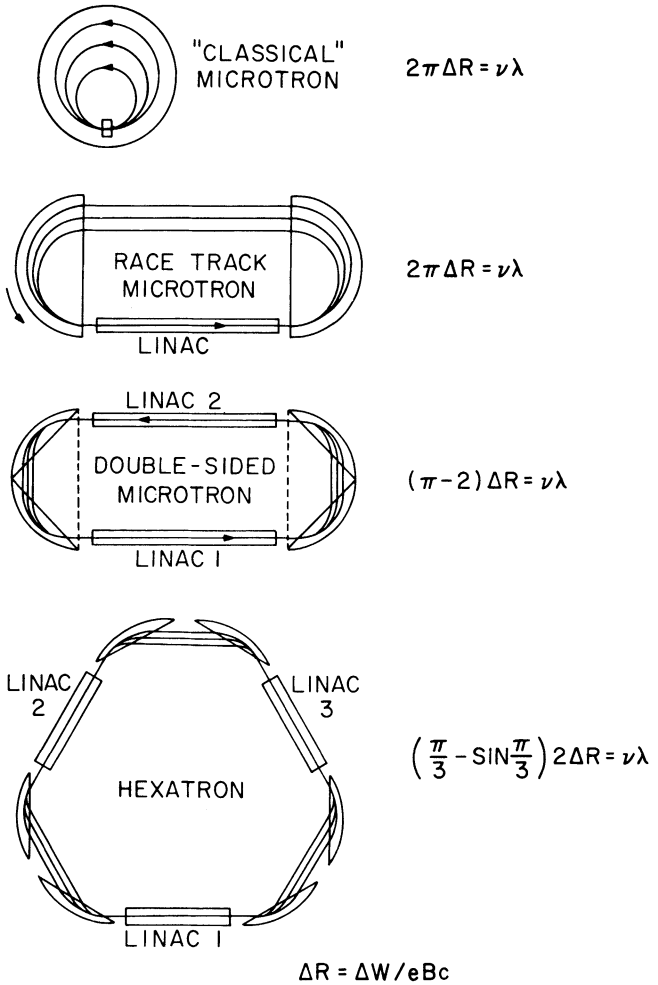

FIGURE 1 Various designs for electron microtrons. The microtron principle states that the increase in length of successive orbits should be an integral number (ν) of rf wavelengths. The resulting restriction on the change in orbit radius ΔR is shown above for each geometry. The condition is met by adjusting the energy gain per turn ΔW and the magnetic field in the sector magnet B to give the prescribed ΔR.

wavelengths. In Fig. 1 the hexatron is compared with other geometries for electron microtrons. In every case the fields in the bending "sector" magnets are assumed to be uniform. The circular geometry of the "classical microtron" corresponds to the design originally proposed by Veksler.[1] The maximum energy attainable in this version is limited by the finite length of the rf cavity. In the racetrack geometry, which was developed to avoid this limitation, the magnetic field is split into two half circular sectors separated by sufficient drift space to allow the insertion of a linac section of substantial accelerating power. This geometry is commonly used to accelerate electrons to energies of a few hundred MeV. For higher energy operation (≥ 500 MeV) the double-sided geometry has been proposed.[2] This geometry is attractive for maximum energies up to approximately 2.5 GeV. For each design the limiting energies result from the increasing mass of the sector magnets, which scales as E^3, and increasingly

stringent conditions on the precision of the $\int Bdl$ over the particle orbits required to insure good beam quality. For higher energies, one must consider a higher-order variant of the microtron geometry such as the Hexatron[3] shown at the bottom of Fig. 1. The basic features of all microtrons derive directly from geometry once an rf wavelength is chosen. By using a six-sided configuration consisting of three linac sections and three dispersive straight sections, one can increase the orbit separation in the dispersive straight sections compared with that possible with the double-sided and racetrack configurations. The smaller bend angle per sector magnet and the lower field in the hexagon geometry can be more easily accommodated with conventional magnet design.

In the CW mode of operation, the quality of the hexatron beam will be unprecedented. Because of the absence of transient modes of rf excitation in the linac, the energy spread in the beam will be limited by the precision of phasing of the various rf accelerating sections. Relative energy spread in the extracted beams will typically be less than 10^{-4}. The limitation in performance of the Hexatron will derive from two sources. Quantum fluctuations in synchrotron radiation will produce significant but acceptable growth in the longitudinal and transverse beam emittance for electron energies above ~ 3 GeV. Below this energy, the geometric quality of the extracted beams will be limited by emittance growth due to the usual aberrations in the guide fields and focusing elements. No significant growth is expected from the extraction process itself. The onset of regenerative beam breakup will limit the maximum current that can be accelerated in the microtron. Extensive analysis of this phenomenon suggests that it will not be present at the operating levels discussed here. Recent experience with a 185 MeV-CW race track microtron[4] provides experimental confirmation of this conclusion.

In the following sections, a complete technical description is presented for a conceptual design of a six-sided CW microtron system. In section 2, the basic operating principles are discussed. The later sections include a discussion of details of the design, the operating characteristics predicted for the Hexatron and options for extending the technology to higher energies.

2. PRINCIPLES OF OPERATION

We begin by developing the basic microtron coherence conditions as they apply to the Hexatron geometry. This requirement on the synchronization of phase of the electron micropulses requires, independent of geometry, that the time taken by an electron to travel along a trajectory from linac exit to linac entrance be an integral multiple of the rf field period. For the Hexatron, this requirement can be written in the form[3]

$$\frac{2(\pi/3 - \sin \pi/3)W_{n,i}}{eBc} + \frac{S_i}{\beta_{n,i}} = \mu_{n,i}\lambda$$

$$\frac{2(\pi/3 - \sin \pi/3)\,\Delta W}{eBc} + S_i\left(\frac{1}{\beta_{n+1,i}} - \frac{1}{\beta_{n,i}}\right) = \nu\lambda, \qquad i = 1, 2, 3 \tag{1}$$

where the index i refers to the first, second, or third superperiod on the nth orbit whose energy is given by W_{ni}. The other parameters are

c = velocity of light
e = electrical charge of the electron

B = magnetic field of bending magnets
S_i = orbit length from exit of ith linac to entrance of next linac in the limit of vanishing electron energy
β_{ni} = normalized electron velocity after the ith linac on nth turn
μ_{ni} = harmonic number for the ith orbit between linacs on the nth turn
λ = free-space wavelength at the fundamental frequency
ν = mode number

In the approximation that $\beta = 1$, the second equation reduces to the coherence condition for the Hexatron

$$\frac{2(\pi/3 - \sin \pi/3)\,\Delta W}{eBc} = \nu\lambda \tag{2}$$

where ΔW is the energy gain per turn. Equation (2) is equivalent to the requirement that successive orbits increase in length by ν rf wavelengths.

The range of phase acceptance and energy spread of the beam in the Hexatron are related to the phase slip per turn $2\pi\nu$. Consider an electron that leaves a linac with a phase error $\delta\phi_k$ and energy error δW_k, where k refers to 1/3 turns through one period of the Hexatron orbit. After the next passage through a linac, the phase and energy errors are respectively

$$\delta\phi_{k+1} = \delta\phi_k + \frac{\delta L_k}{\beta_k\lambda}\,2\pi \tag{3a}$$

$$\delta W_{k+1} = \delta W_k + eV_0[\cos(\phi_s + \delta\phi_{k+1}) - \cos\phi_s], \tag{3b}$$

where V_0 is the peak linac voltage and ϕ_s is the synchronous phase. Note that the energy gain per turn is given by

$$\Delta W = 3eV_0 \cos\phi_s \tag{4}$$

Substituting

$$\delta L_k = \frac{2(\pi/3 - \sin\pi/3)}{eBc}(\beta_k\delta W_k + \delta\beta_k W_k)$$

$$\approx \frac{2(\pi/3 - \sin\pi/3)\beta_k\delta W_k}{eBc}$$

in Eq. (3a), neglecting higher-order terms of $\delta\phi_{k+1}$ in Eq. (3b) and using Eq. (2a), we obtain, after some manipulation

$$\delta\phi_{k+1} = \delta\phi_k + \frac{2\pi\nu}{\Delta W}\delta W_k$$

$$\delta W_{k+1} = \delta W_k - eV_0 \sin\phi_s\left(\delta\phi_k + \frac{2\pi\nu}{\Delta W}\delta W_k\right)$$

or in matrix form

$$\begin{pmatrix} \delta\phi_{k+1} \\ \delta W_{k+1} \end{pmatrix} = M \begin{pmatrix} \delta\phi_k \\ \delta W_k \end{pmatrix} \tag{5}$$

where

$$M = \begin{pmatrix} 1 & \dfrac{2\pi\nu}{\Delta W} \\ -eV_0 \sin\phi_s & 1 - \dfrac{2\pi\nu}{\Delta W} eV_0 \sin\phi_s \end{pmatrix}.$$

Since the determinant of M is equal to one, the motion is stable if the trace of M satisfies the condition

$$-2 < 2 - \frac{2\pi\nu}{\Delta W} eV_0 \sin\phi_s < 2$$

or more fully, using Eq. (4)

$$0 < \tan\phi_s < \frac{6}{\pi\nu} \tag{6}$$

For $\nu = 1$, which pertains to the design discussed here, the region of stable synchronous phase extends over rf phase angles from 0 to 62.4 deg. For comparison, in a racetrack microtron operating in a mode with $\nu = 1$, the corresponding region of stability is 0 to 32.5 deg.

The ellipses that characterize particle motion in longitudinal phase space are upright in the middle of the linacs and in the dispersive drift spaces between the sector magnets. The energy spread of the beam is given by

$$\begin{aligned} \delta W_{\max} &= \sqrt{\frac{\tan\phi_s}{6\pi\left(1 - \dfrac{\pi}{6}\tan\phi_s\right)}}\, \Delta W \delta\phi_{\max} \text{ (dispersive section);} \\ &= \sqrt{\frac{\tan\phi_s\left(1 - \dfrac{\pi}{6}\tan\phi_s\right)}{6\pi}}\, \Delta W \delta\phi_{\max} \text{ (center of the linac),} \end{aligned} \tag{7}$$

where $\delta W_{\max}$ is the maximum energy deviation from the synchronous energy for bunch motion in $\delta W \delta\phi$ space for which the corresponding maximum phase difference from ϕ_s is $\delta\phi_{\max}$, and ϕ_s is the stable phase angle.

For the design values cited in the next section, $\phi_s = 18°$, $\Delta W = 105$ MeV, and for a phase-space area of 30π keV-deg the maximum energy and angular spreads will be ± 90 KeV and ± 0.34 deg in the dispersive straight sections and ± 81 KeV and ± 0.37 deg at the linac centers.

3. CHOICE OF BASIC ACCELERATOR PARAMETERS

The basic parameters that specify a given Hexatron design are the rf wavelength λ, the energy gradient in the linac V_0, the energy gain per turn by a synchronous particle ΔW, the injection energy E_0, and the drift distances that characterize the lowest-energy orbit. The rf frequency must be high enough to insure that the microstructure of the individual external beams has a period comparable to or smaller than the resolving time typical of experimental instrumentation, $\tau \approx 1$ to 2 nsec. In our case, this condition is met by use of S-band, $\lambda = 0.125$ m rf waveguides in the Hexatron linacs. The choice of V_0 is a compromise between capital cost for the three linac sections and the advantages of minimizing the drift distances that separate the sector magnets in the nondispersive straight sections. Current economics of cw linac design imply a cost optimum value for V_0 of 1.0 to 1.2 MeV/m. In our design, we have chosen 1.5 MeV/m. The value of ΔW is also constrained by the value of the magnetic field in the sector magnets. The basic coherence condition, Eq. (2), fixes ΔW for a given value of B once the mode number is chosen. In the ANL design $\nu = 1$ is chosen in order to maximize the region of rf phase stability. The sector magnet field was taken to be 1.0 Tesla to insure good field quality. These choices fix the value $\Delta W = 105$ MeV.

The remaining choices of drift distance and injection energy are largely a matter of convenience. The injection energy of 185 MeV was chosen to correspond to the racetrack design currently under construction.[5] With the drift distance S_i defined as in Eq. (1), the initial synchronism condition becomes

$$S_i + \left(\frac{\pi}{3} - \sin\frac{\pi}{3}\right) 2\rho_{ni} = \mu_{ni}\lambda \tag{8}$$

The Argonne design is characterized by the parameters $\mu_{11} = \mu_{12} - 1/3 = \mu_{13} - 2/3 = 250$. The long straight sections in which the linacs are located are 28.00 m in length. The phase of the rf in each of the linacs will be adjusted to accommodate the path-length difference in the successive superperiods of each full orbit arising from the corresponding 35-MeV energy difference. The dispersive straight sections between the sector magnets are a minimum of 5.26 m and a maximum of 26.98 m, allowing space for the quadrupoles and other elements necessary for operation of the machine.

A tabulation of the basic parameters for the conceptual design discussed in this paper is presented in Table I. These choices are discussed in more detail in the next section.

4. DESIGN OF A 4-GeV HEXATRON

A. Introduction

The GeV Electron Microtron (GEM) design discussed here is a three-stage cascaded system of accelerators. The basic configuration shown in Fig. 2 consists of a 23 MeV cw linac injector, a 185-MeV booster racetrack microtron and a hexagonal microtron system. We will focus discussion solely on the third stage, the Hexatron. The first and second stages involve state-of-the-art technology. The reader is referred to references[6–9] for information on the detailed design and performance of these systems.

The beam extracted from the racetrack microtron (RTM) will be injected into the Hexatron in a dispersive straight section at 185 MeV. The beam is accelerated to the maximum energy in 109 passes or 36–1/3 turns. The synchronous particle gains

TABLE I

ANL Hexatron Design Parameters

Maximum Energy	4000 MeV
Injection Energy	185 MeV
Current	300 μA
Energy Spread, $\Delta E/E$	$\approx 10^{-4}$
Beam Emittance	≤ 0.2 mm-mr
Magnetic Field	1.015 T
Maximum Orbit Radius	13.145 m
Minimum Orbit Radius	0.608 m
Energy Gain Per turn	105 MeV
Rf Wavelength	0.125 m
Mode number, ν	1
Synchronous Phase	$18°(\nu_s \approx 0.4)$
Longitudinal Stability Limit	62.4°
Ave. Acceleration Field	1.46 MV/m
Energy Gain Per Linac	35 MeV
Number of Linacs	3
Length of Linacs	24 m
Shunt Impedance, ZT^2	68 $M\Omega$/m
Rf Power Losses	3.1 MW
Length of LSS	28 m
Length of DSS for $E_e = 0$	28 m
Minimum Length of DSS	5.26 m
Orbit Separation in DSS	0.1725 m
Orbit Length Increase Per Turn	$3\lambda = 0.375$ m
Maximum Number of Recirculations	109/3

35 MeV energy in passing through each linac. Each orbit in each of the three dispersive straight sections contains a quadrupole focusing structure. Two focusing configurations are described in this section. Both schemes assume no focusing in the linacs themselves. Figure 3 shows the Hexatron layout for one-third turn. The linac centers are indicated at points A and E. The distance to the effective dipole edges are $d = 14.0$ m. One configuration uses a relatively weak doublet system composed of a horizontal focusing quadrupole and a horizontal defocusing sector magnet edge angle at the ends of the linac sections. The second configuration uses a much-stronger two-quadrupole doublet system at these locations. The dipole exit edges are located at points B and D. The focusing system in the dispersive straight section is mirror symmetric about the midpoint C. The optical transformation from points A to E should be first-order achromatic in the bend plane ($\eta_A = \eta_E = \eta'_A = \eta'_E = 0$), and waist to waist in both transverse planes with ($\beta_A = \beta_E$, $\alpha_A = \alpha_E = 0$), where α and β represent the usual Courant-Snyder parameters from accelerator theory. Since the numbers of quadrupoles, field strengths, and locations are all variable, a large set of solutions can be found that satisfy the constraints on α_x, α_y, η, and η'. The solutions presented here may not be optimum, but some effort has been expended to ensure that the behavior of the β_x, β_y, and η functions is reasonable with respect to sensitivity to quadrupole strengths and beam size and dispersion.

B. Transverse Optics

To eliminate the first-order horizontal-longitudinal phase-space coupling, the dispersion function η must be zero in the linac straight sections. The horizontal and vertical matched waist sizes at the centers of the linac sections have been chosen to be 15.0 m, a

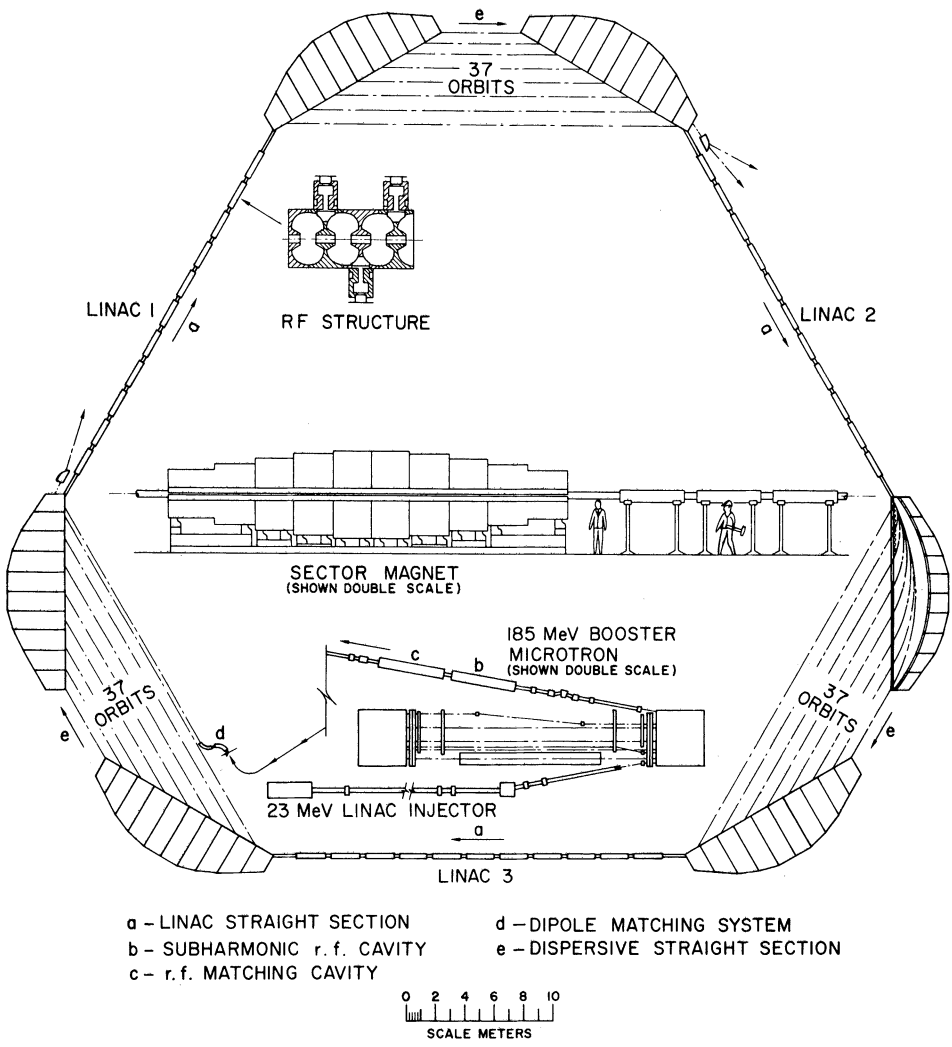

FIGURE 2 Schematic of the Argonne National Laboratory 4 GeV Electron Microton-GEM. The accelerator is a six-sided microtron consisting of three dispersive straight sections and three dispersion-free straight sections in which three linacs are located. Also shown is a 185 MeV racetrack booster microtron which serves as an injector. The energy gain per linac is 35 MeV giving a gain of 105 MeV per turn. Three 100-μA beams can be extracted as indicated at the exit from dispersive straight sections. The injection beam line between the booster and Hexatron and placement of the booster are not shown.

value close to the optimum value of 14.0 m for the 28.0 m length of the linac straight section. Since the focusing systems for each energy have mirror symmetry about the centers of the dispersion sections, the focusing elements in these sections must be adjusted to produce transverse waists ($\alpha_x = \alpha_y = 0$) and zero dispersion function slope ($\eta' = 0$) at these points, i.e., at point C in Fig. 3. The dipoles are assumed to bend the beams through 60° with an effective length $\rho\pi/3$ where ρ is the radius of curvature. The edge-focusing terms are modified to correspond to a short-tail drop off of the central field.[10] In the horizontal plane, the dipole edges correspond to thin lenses of power $= +\tan\theta/\rho$. The vertical-plane focusing is modified by the short-tail field

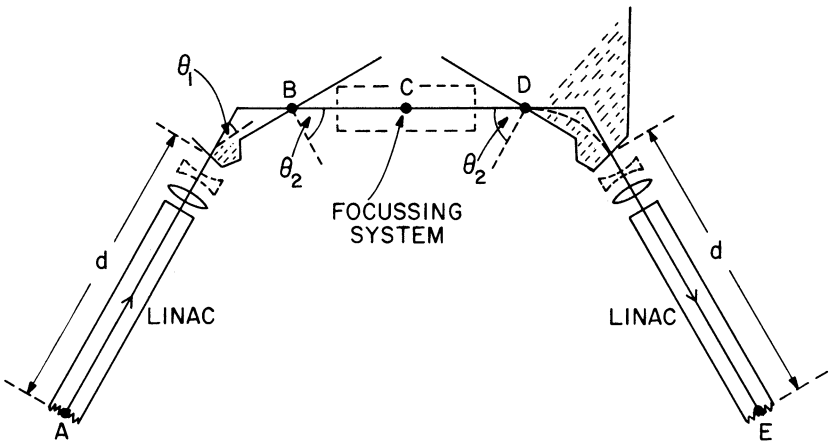

FIGURE 3 Hexatron layout for one-third turn. In the present design, $d = 14$ m. The dotted quadrupoles are used in an alternative focusing scheme described in the text in which the dispersive edges of the sector magnets are not stepped, and θ_1 is zero degrees.

behavior and can be represented by thin lenses of power $= -\tan\bar{\theta}/\rho$, where the effective edge angle $\bar{\theta}$ is determined from calculations by Enge.[10] The solutions given here constitute matched systems for each 1/3 turn assuming constant energy; the energy is increased by 35 MeV between 1/3 turns.

In the first solution, the singlet quadrupole adjacent to the linac is chosen to have a strength $P_s = 0.15\ \text{m}^{-1}$ at 185 MeV (horizontal focusing). The entrance dipole angle θ_1 is taken at $+15°$ (vertical focusing). The exit dipole angle is maintained at 0° at energies $W \leq 1620$ MeV by means of steps in the magnet to reduce the severe vertical defocusing that would result at low energy from the $-60°$ exit angle (used for $W \geq 1655$ MeV).

In the first solution, three quadrupole focusing systems have been developed to contain the electron orbits over the energy range of 185–4000 MeV. Each system is mirror symmetric about the center point C. For $W \leq 1620$ MeV, six quadrupoles between points B and D are used; the dipole exit angles are stepped to zero degrees in this case. A triplet is used for $1655 \leq W \leq 2215$ MeV; for $W \geq 2250$ MeV, five quadrupoles are used. The thin-lens equivalents of the three systems are illustrated in Fig. 4, together with the trajectory of the dispersion ray. Focusing lenses are horizontal focusing (HF). At points B and D, $\eta = \rho/2$ where $\rho(= 3.2855\ \text{E m/GeV})$ is the radius of curvature in the sector magnets. The slope of the dispersion ray at point B is $\eta'_B = \sin 60°$ for system I, where the exit entrance angle is zero degrees ($\theta_2 = 0$); $\eta'_B = 0$ for systems II and III. The length of the dispersive straight section $d_{BD} = 2d_{BC} = 2 \times (14.015 - \rho \times 0.866)$. Figure 5 shows the energy dependence of the resulting quadrupole strengths in the focusing systems–the abscissa is in units of 1/3 turns corresponding to $\Delta W = 35$ MeV. The discontinuities occur at the transition points between focusing systems. Note $P_1 \equiv 0$ in system II.

The conditions of zero dispersion in the linac sections and mirror symmetry cause the horizontal linac to linac phase advance σ_x to depend (to within $2\pi n$, n an integer) only on the linac center waist size β_A, and the linac section focusing elements. In fact

$$\tan \sigma_x/2 = -\frac{\beta_A(A_{11}\sqrt{3} + \rho A_{21})}{(A_{12}\sqrt{3} + \rho A_{22})}, \tag{9}$$

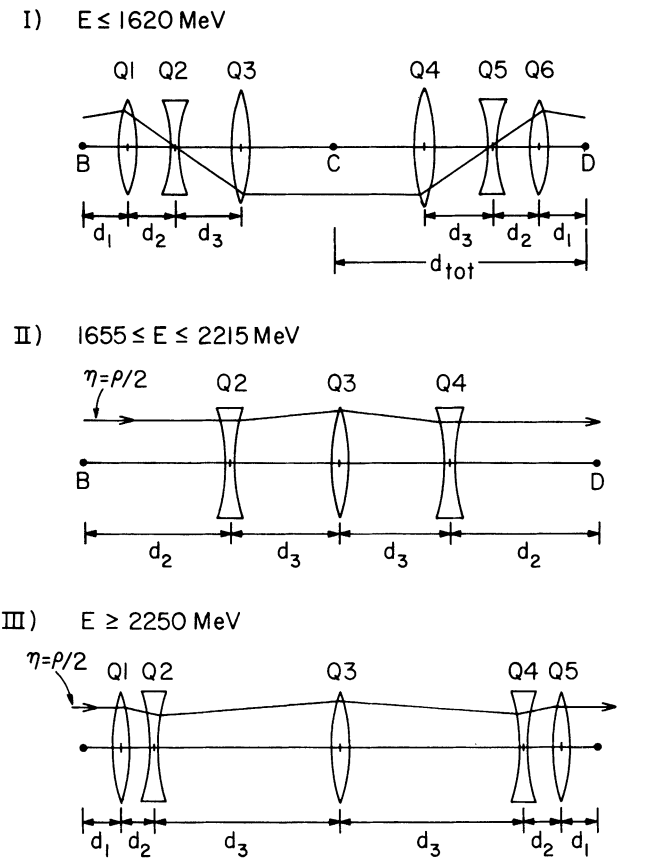

FIGURE 4 Thin-lens representation for the three focusing systems used in the Hexatron in the dispersive straight sections for orbit containment.

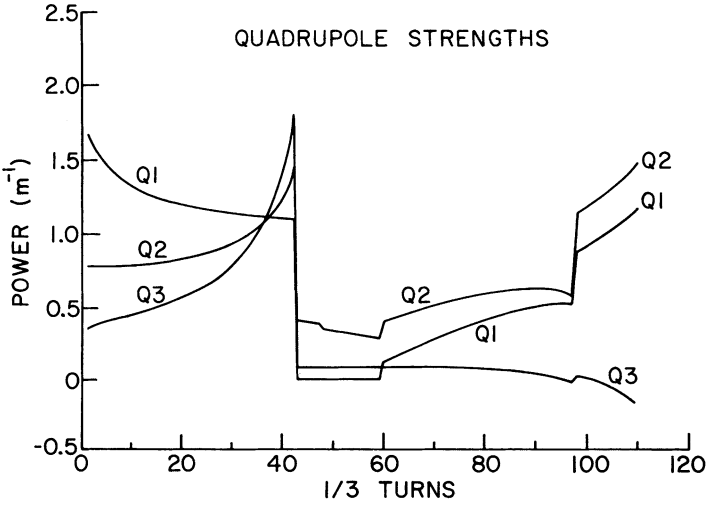

FIGURE 5 Quadrupole strengths proposed for Hexatron orbit containment.

where A_{ij} are the components of the linac center-to-sector-magnet horizontal transformation matrices. Since all energy beams share the same linac section focusing elements, the matrix components depend on the energy. For the focusing elements in configuration I and $\beta_A = 15.0$ m, an expansion of Eq. (9) gives for the leading terms

$$\sigma_x = (0.739 + 0.0195E + n)2\pi \qquad (E, \text{GeV}) \tag{9a}$$

In region I, $E \leq 1.62$ GeV, the type of match achieved with the dispersion section quadrupoles gives $n = 1$. For all solutions at $E > 1.62$ GeV, $n = 0$.

The vertical phase advances are less constrained and are dependent on the dispersion-section matching conditions. The values range from 0.8π at low energies to about 1.7π at the highest energies. Figure 6 shows the energy variation of β_x and β_y for three points: the dispersion-section dipole end, at Q_2, and at Q_3. At injection β_x is large (≥ 120 m) in Q_3 and decreases rapidly with energy. The values of β_y in Q_2 rise to about150 m near the end of region I.

The second configuration, which does not require steps in the sector magnets, can be used for the transverse optics of Hexatron. While the elimination of these steps would provide negligible savings in fabrication (less than 1% of sector magnet cost), significant savings should be encountered in shimming, tuning, and operating the magnets, reducing the required development costs. This configuration includes two

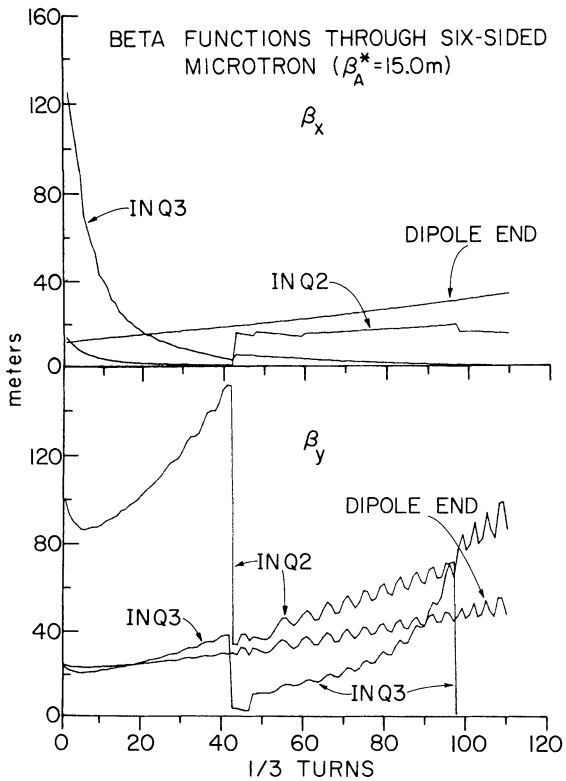

FIGURE 6 Beta functions in the hexatron ($\beta_A^* = 15.0$ m) at three fixed points plotted as a function of successive 1/3 turns.

quadrupoles at each end of the linac tuned to focus the beams to waists at the dispersive edge of the following sector magnet at low energies. The solution presented below is offered only as an existence proof and have not been carefully optimized. Nevertheless, it shows the following features: 1) all energies 0.185 – 4.0 GeV can be focused without using quadrupoles of unusual dimension or strengths; 2) the β_x, β_y functions are reasonable (<100 m) for all energies, implying reasonable sensitivity to quadrupole strengths; 3) the η functions are of comparable size to the solution presented in the earlier design (Ref. 6) and could be further reduced by the addition of quadrupoles in the lowest beam lines; and 4) the number of quadrupoles required is not significantly greater than in the first configuration discussed above. Magnet aberrations due to sector-magnet fringe fields have been minimized by using normal incidence and β_x, $\beta_y < 25$ m at the linac end of the sector magnet, and a very small waist $\beta < 1$ m at the sector-magnet exit for low-energy orbits.

The optical system in this second solution includes a quadrupole pair between each linac and sector magnet. These quadrupoles have powers ($B'l/B\rho$) of 1.26 m^{-1} and 1.62 m^{-1} (horizontally focusing and defocusing, respectively) at 185 MeV. The horizontally focusing and defocusing elements are 1.00 and 0.55 m from the sector-magnet edge respectively. The beam enters the sector magnet from the linac at normal incidence, i.e. $\theta = 0°$. The lengths of the quadrupoles are 0.30 m. The sector-magnet edges at the dispersive section ends have horizontally focusing edges of 60°. The basic configuration for the quadrupoles in the dispersion straight section for orbits below 1.8 GeV is shown in Fig. 7, together with the quadrupole strengths. Since the beam is

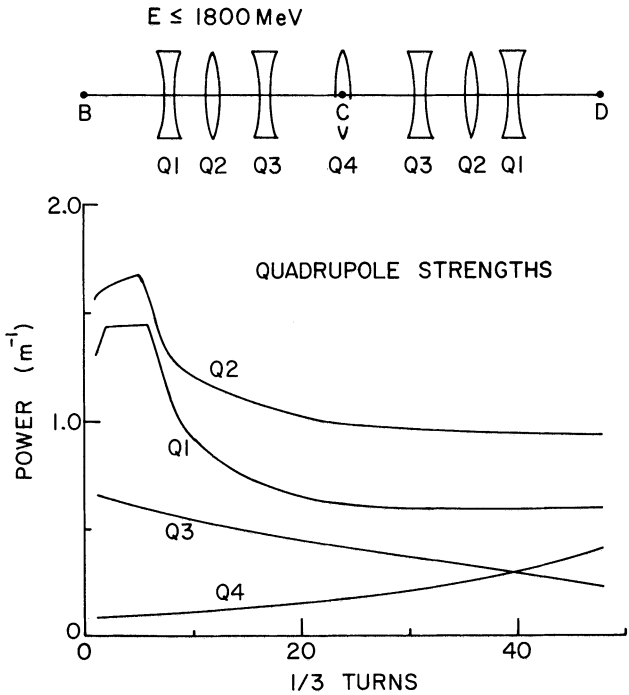

FIGURE 7 Thin-lens representation of the focusing system used in the Hexatron with sector magnets without shaped edges, and corresponding quadrupole strengths for orbits with energy less than 1.8 GeV.

focused very tightly at the 60° exit/entrance of the sector magnets, the effect of edge-angle focusing is minimized and the constraints on the optics of the dispersive straight section are similar to those using a stepped magnet. The solutions above 1.8 GeV are almost identical to those without steps.

C. Sector Magnets

One of the major challenges of the Hexatron concept is the design of the sector magnets, which must provide guide fields with the required profile, precision, and stability. In a design of a six-sided system using conventional straight-edge magnets, the entrance and exit angles for each orbit relative to the normal field boundary are 60°. Strong vertical edge defocusing forces result, particularly on the low-energy orbits. The two systems of transverse optics discussed in the previous section were developed to compensate for these forces. In the solutions 1 and 2 discussed above, the pole-face edge at the non-dispersive end of each sector magnet is rotated to near-normal or normal incidence, respectively. In addition, in the first case, stepped edges are used for the low-energy orbits to eliminate these forces on the dispersive edge of each sector magnet. In the second case a solution of transverse optics was found that provides a waist near the dispersive edge of the sector magnet on the low-energy orbits, minimizing sensitivity to edge-angle focusing. In this second case, the dispersive edge is not stepped. The detailed design of the stepped sector magnet presented in this section was developed to demonstrate scientific feasibility. The information from this effort similarly provide direct confirmation of the feasibility of the simpler unstepped sector magnet required for the second design option.

Basic design. The design values of the central magnetic-field strength, the maximum electron energy, and the 60° orbit bend angle determine the overall dimensions of the field region. For a nominal central field strength of 1.015 T and 4-GeV operation, the chord length of the sector magnet gap is 13.4 m, the maximum pole piece depth is 1.84 m and the outer radius of the field region is 13.22 m. The basic geometry along the chord of the stepped sector magnet edge using shaped edges is shown in Fig. 8 with plane and isometric views of the edge of the magnet. The pole edge contains steps for 14 orbits on the low-energy end of the chord and is straight at the high-energy end. In the unstepped option, the low-energy end of the magnet is identical to the high-energy end.

The design goal for the uniformity of the integral of the magnetic field along each beam orbit is one part in 10^4. Fluctuations of this magnitude in the integral from one orbit to another will induce synchrotron oscillations with maximum amplitudes measured relative to beam energy of 10^{-4}. Two major factors contribute to these fluctuations. The first is errors in the central field strength and the second is the softness of the field edge. Two-dimensional TRIM[11] calculations for an average radial section through the sector magnet show an uncorrected central-field variation of 5×10^{-3}. By incorporating a 0.3 cm thick, parallel homogenizing gap, i.e., a "Purcell Filter," into the magnet design, as shown in Fig. 9, this variation can be reduced to about one part in 10^3. The Purcell gap is located outside the end guard and has a separate coil driving it. This coil is connected in series with the main coil, but can be independently adjusted over a small range of currents to minimize the flux leakage from the end guard. Steel shims or trim coils can be inserted into the magnet gap and Purcell gap near the pole edges to provide additional flattening. Shims and trim coils in the Purcell gap and pole face windings in the main magnet gap will be used to provide additional field flattening.

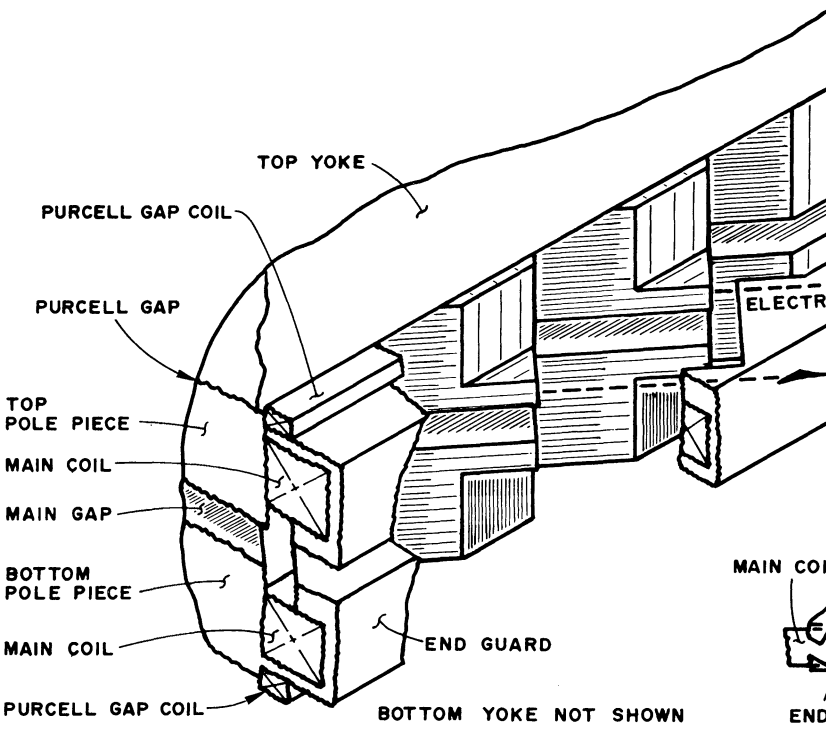

FIGURE 8 Plane view and isometric representation of the area of the chord edge of th
profile changes to the straight edge. Magnetic shims at the pole edges and shield plates at t

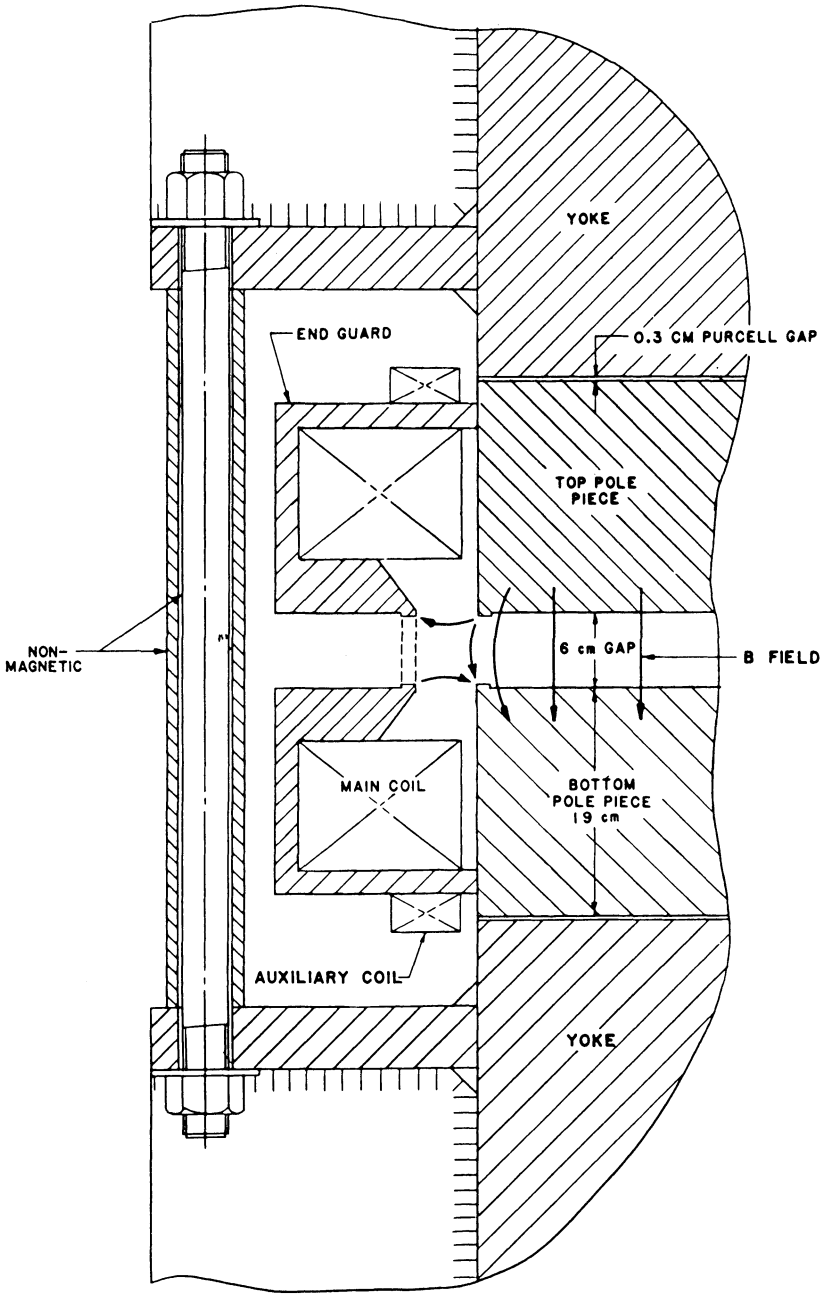

FIGURE 9 Cross section through the chord edge of a sector magnet in the high-energy end. Minor non-magnetic support structures are not shown.

In order to maintain phase stability for electrons of widely differing energies ($E_{max}/E_{min} = 21$), one would like to ensure that $\Delta s/\Delta \rho$ is a constant independent of particle momentum. This is easiest with a sharp magnet edge and one means to do this is an end-guard geometry as shown in Fig. 9. The end-guard dimensions and coil currents are adjusted so that the field between the end-guard plates is as small as possible. Low fields are produced in the end-guard region when the fringe field from the pole tips is cancelled by the return field around the outside of the excitation coils, producing a separatrix in the median plane about one gap width from the edge of the pole tips. The end guards can be joined by shield plates across the gap and these shield plates will not be saturated if the proper geometry and current ratios are maintained. Additional shims can be used to produce the hardest edge possible. These are located at the edges of the pole tip and end guard.

In order to develop supporting evidence for the feasibility of the shaped-edge design of the sector magnet, a full-scale prototype magnet that replicates the three lowest-energy orbits in the sector magnets was built. Details of the design are presented elsewhere.[12] Measurements were made on this magnet and three-dimensional magnetostatic field calculations were made using 1010 steel elements arranged in exactly the same geometry as the prototype. The measurements have been made without and with one set of steel shims at the edges of the poles. The three objectives of this endeavor were to show that: 1) the field profile along the beam path falls off at least as sharply as the Enge short-tail edge, 2) the field contours can be oriented within about 5° to be perpendicular to the beam paths, and 3) contributions of higher-order multipoles of the field are small and controllable. The calculations on this magnet used the proprietary 3D magnetostatic program TOSCA,[13] which was developed at the Rutherford Appleton Laboratory. The resulting vertical field calculations were analyzed in the same manner as the measured data.

The field profiles are shown in Fig. 10 for a line along the exterior beam path. A plot of an Enge short-tail is also shown for comparison. The plots clearly show that all

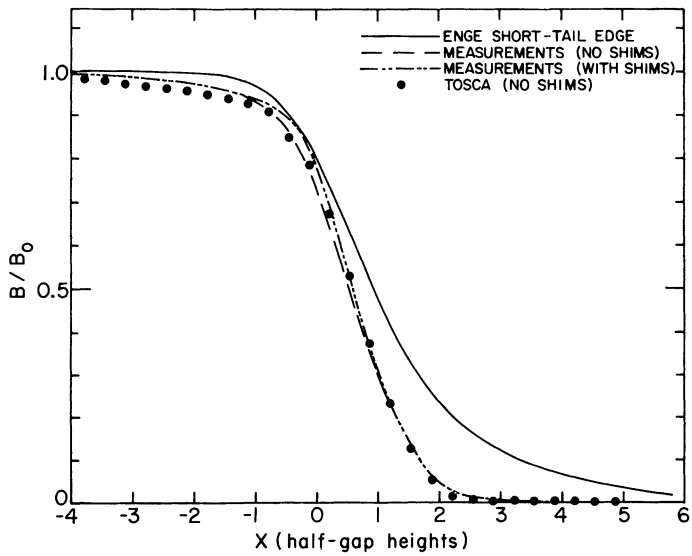

FIGURE 10 Plots of calculated and measured edge-field profiles for the hexatron sector magnets.

calculations and measurements on this magnet fall off considerably more sharply than the Enge short-tail field. The angles of the field contour lines agree well with the predictions[14] of TOSCA for the unshimmed magnet. Preliminary studies of shimming of a 2/3-scale prototype[12] show that quadrupole gradients can be reduced to acceptable values.

Support and alignment. Surveying of the accelerator could be done relative to a large equilateral triangle with survey monuments as shown in Fig. 11. This would eliminate closure errors and minimize the distances required in secondary measurements. Following developments at CERN,[15] it seems possible to make all measurements of length using laser interferometry (which can be accurate to $\Delta x/x \sim 10^{-8}$). Height measurements can be done with a capacitive readout on a mercury liquid level (which should be accurate to $\pm 2.5\ \mu$ over the distances involved).[16] In order to ensure maximum accuracy, it seems desirable to use evacuated or sealed temperature-controlled tubes for distance measurements. Invar wires could also be used for specific distance measurements. Using these techniques, magnet positions should be known very quickly within 20–30 μ.

Maintaining alignment in the presence of settling and thermal fluctuations should be relatively straightforward. Since the thermal-expansion coefficient (C_T) for iron and concrete is of order $1 \times 10^{-5}/°C$, thermal effects can be easily controlled. It would be

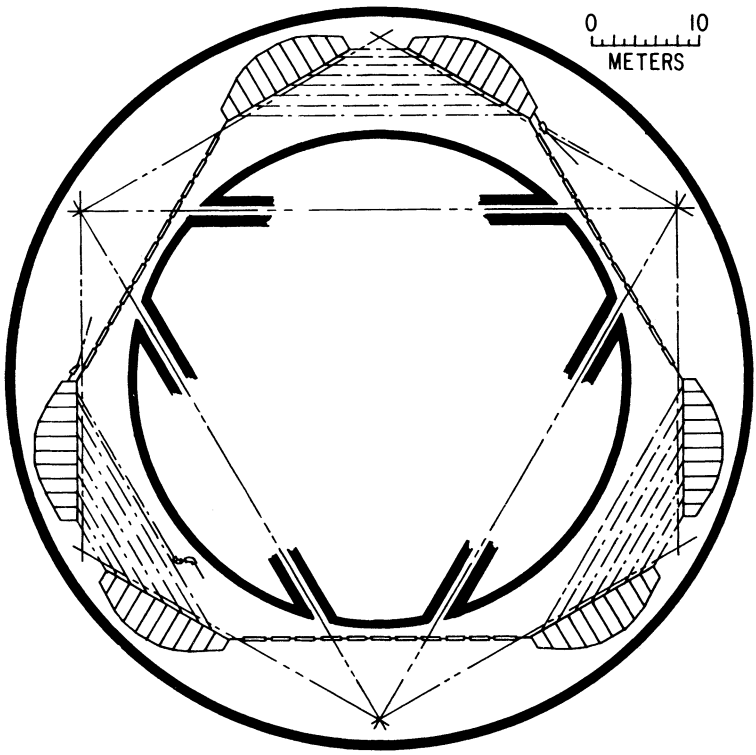

FIGURE 11 Survey grid proposed for alignment of Hexatron components.

desirable to have the temperature of major structural components be constant to

$$\Delta T = \frac{\Delta x}{C_T L} = \frac{\pm 0.3 \times 10^3}{10^{-5}\, 30} = \pm 1^\circ C$$

This could be insured by using insulation and good thermal contact to constant-temperature baths. Alignment could be maintained by mounting critical components on a number of jacks that could be remotely controlled in three axes in small increments. Support of sector magnets could make use of CERN-developed polyurethane jacks[15] modified to support extra weight by using larger support areas. Since horizontal displacement is also critical, these jacks might also be used to accomplish horizontal motion. Although the weight of the sector magnets is considerable (675 tons), these magnets are only 12% heavier than the ZGS octant magnets that occupied the ZGS ring area where the Hexatron would be located for 15 years. Survey data on ZGS magnets showed that ZGS octants settled at a rate of about 0.15 mm/year. This settling rate is about one half of what the computer-control system conservatively could handle; therefore, resurveys on an annual basis would maintain adequate alignment. On-line level sensing and correction systems capable of maintaining level errors comparable to readout errors of the mercury levels are, in principle, possible. Horizontal errors could also be reduced by means of on-line sensing and correction systems.

D. Hexatron rf System

High rf efficiency is one of the primary requirements governing the choice of accelerating structure for the Hexatron. Various geometries for cavity structures characterized by high shunt impedance have been investigated because of their potential for improved efficiency. The most successful of these is the side-coupled cavity geometry[17] developed at Los Alamos National Laboratory for the LAMPF accelerator. The optimization of this geometry led to a clear advance in conversion efficiency of rf to beam power. More recently two designs, the on-axis coupled structure[18] and the Andreev disc and washer structure[19] have been studied extensively. The disc and washer structure shows promise for attaining the highest shunt impedances. Early enthusiasm for this structure was dampened somewhat by the discovery of an overlap between the operating frequency and a TM_{11}-like passband, known as the deflecting-mode passband. Recently, however, Iwashita[20] has found that the washer supports can be modified to provide an effective means of modifying the TM_{11} passband so that it no longer crosses the operating frequency. Subsequent experimental data described below have confirmed these theoretical predictions. The on-axis coupled structure is shown in cross section in Fig. 12. This geometry has several advantages that make it an attractive choice for the hexatron. Fabrication is simplified because of the coaxial geometry and, because the coupling cavities are in line, the overall radius of the structure is less than other geometries. Excitation of transverse deflecting modes can be suppressed by splitting the resonance frequencies for HEM_{110}-like modes. This is accomplished by rotating[21] the coupling slots that connect adjacent cavities. Recent developments have made the choice of acceleration structure somewhat easier, as side-coupled, disc and washer, and on-axis-coupled all seem acceptable.

The frequency of the cavity design for the Hexatron is f = 2.4 GHz with $\beta = 1$. An effective shunt impedance (ZT^2) of 67.5 MΩ/meter with a 1.6 cm beam aperture is

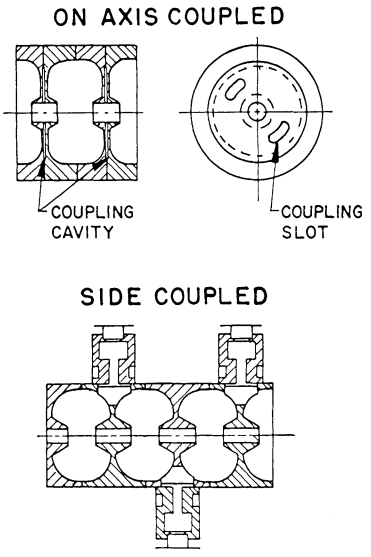

FIGURE 12 Design options for rf cavity structure in Hexatron linacs.

expected on the basis of measurements of existing side-coupled[22] and on-axis-coupled[23] structures. Again, recent results on the LASL-NBS linac have shown these parameters can be obtained on the side-coupled linac structure with very high power dissipation (48.5 kW/m). The side-coupled structure can be operated at a gradient of 1.81 MeV/m with a synchronous phase $\phi_s = 18°$, resulting in an accelerating field of 1.72 MeV/m. The rf power input will be 45 kW/m for the accelerating fields and 16.8 kW/m for beam loading. This performance reflects the high efficiency of cooling and freedom from detuning at high power that results from the basic geometry of the side-coupled structure. The on-axis-coupled structure has the advantage of higher cell-to-cell coupling. But the power dissipation of 45-50 kW/m or 2.9 kW per cavity is relatively high and there is concern that even with maximum possible water cooling in the periphery of the beam aperture, the on-axis-coupled cavity structure might detune (i.e., as a result of thermal deformation the frequencies of the main cavity and the coupling cavity may separate).

The accelerating structures for the Hexatron linac can be built in 2.06 meter sections with eleven sections per linac. The 5 to 10% coupling factor of the on-axis-coupled cavities and the 4.7% of the side-coupled cavities are considered adequate for this length. Power would be fed into the center of the structure through an rf coupler connected by flanges to two 1.03 m sections. The geometry of the present design permits the addition of 2 cells per linac section or the addition of one and one-half linac sections to decrease the accelerating gradient if that should prove necessary to provide higher acceleration gradients or reduce power dissipation in the wave guide.

RF power at $f = 2.4$ GHz can be provided by cw klystrons. At least one Thomson C.S.F. TH 2075 is presently operating in the Mainz microtron, MAMI-I and in many industrial applications. It delivers a minimum of 50 kW of rf power and its operating efficiency is 62%. For 4 GeV operation, the Hexatron linacs could use 22 TH 2075 klystrons each for a total of 66. Two klystrons in parallel would be coupled directly through a combiner to each 2.06 m waveguide section. A feedback loop to one klystron

in each section can automatically maintain constant accelerating field. The phase of the individual rf sections can be controlled to within 1 degree with a closed feedback system that controls the phase of the drive. No recirculators or high-power mechanical phase shifters would be used in normal operation. The total rf power required at 4 GeV would be 3,950 kW, including 400 kW for the injector and 200 kW for the RTM. A total of 78 klystrons would be used, requiring 6.3 MW of dc power at 25 kV in 4 GeV operation.

5. MULTIPLE-ENERGY EXTRACTION FROM THE HEXATRON

One of the inherent features of microtrons is the ease with which the beam can be extracted with negligible deterioration of beam quality. This is possible because beams of different energies occupy different orbits in the dispersive straight sections. Insertion of a modest-field deflection magnet on any energy orbit in any dispersive straight section will cause a displacement of the beam after passing through the next sector magnet in the next linac straight section. A septum magnet placed downstream of the sector magnet and upstream of the linac will further deflect the displaced beam to miss the linac. Extraction is possible from any orbit.

The versatility of the microtron can be enhanced if the circulating beam can be split so that selected fractions can be extracted on specific orbits. In this manner, simultaneous extraction at multiple energies can be realized. This can be accomplished by inducing an energy structure on the micropulse train. Because the different energy pulses will be horizontally separated in the dispersive straight sections, septum deflectors can be used to extract specific fractions of the beam on given orbits. The energy structure can be imposed by subharmonic modulation of the individual micropulses prior to injection into the microtron. In the GEM design, three separate energy beams are extracted. A 1/3-subharmonic cavity operating at 800 MHz is located in the beam line between the RTM and the hexatron. The rf phase of the cavity is adjusted to give three sets of bunches A, B, and C with energies $W_i + \delta W_i$, W_i, and $W_i - \delta W_i$, respectively. The upper drawing of Fig. 13 shows the location of these bunches relative to the linac and sub-harmonic cavity rf phases. The beam is injected into the lowest-energy dispersive section through a system of quadrupoles and dipoles designed to produce a phase shear of $\delta\phi_i = -0.4332\ \delta W_i/\text{MeV}$. Therefore the pulses A, B, and C are injected with phase angles $\phi_i + \delta\phi_i$, $\phi_i - \delta\phi_i$, respectively.

As shown at the bottom of Fig. 13, the rf focusing will cause the pulses displaced in energy to oscillate about the zero-energy error pulses, 180° out of phase with each other. At selected energies determined by the synchrotron-oscillation frequency (the design value is 0.406 per revolution), one of the displaced pulses will have nearly its maximum energy error, $\delta W_{\max}$, in a dispersion straight section. It will therefore be horizontally separated from the other two pulses and can be extracted by a septum deflection system. The linac voltage can be varied slightly to adjust the synchrotron frequency so that the maximum-energy excursion can be made to occur on any desired orbit. Once either the lowest or intermediate extracted-beam energy has been chosen, the possible energies for the other beam are somewhat restricted. The highest-energy beam can of course be extracted at any energy higher than the intermediate energy.

The energy displacement $\pm\delta W_i$ supplied by the subharmonic cavity is determined by the required value for $\delta W_{\max}$, the phase-angle shear of the injection line downstream of the cavity and the longitudinal focusing conditions in the Hexatron. For the design values, the result is $\delta W_i = 0.15\ \delta W_{\max}$.

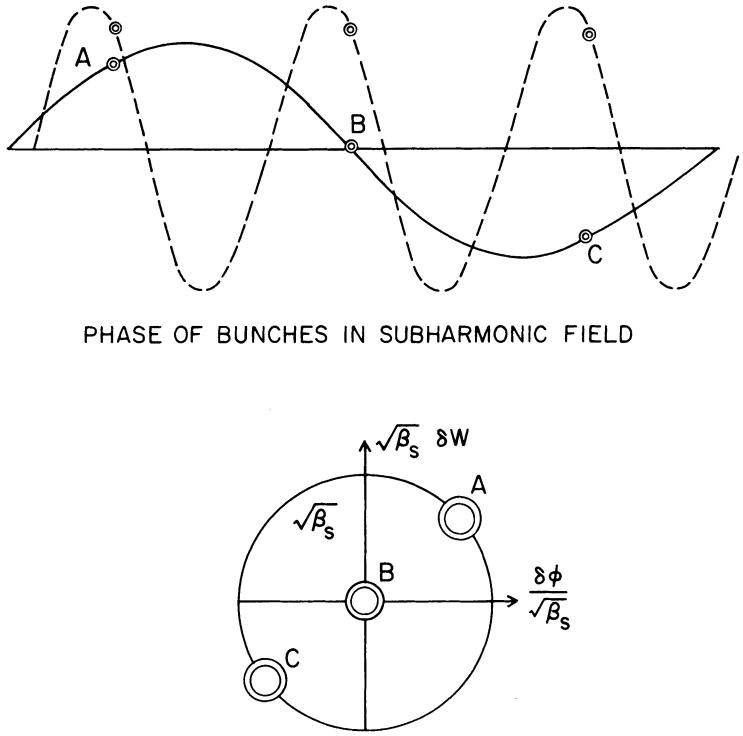

FIGURE 13 Generation of bunch-to-bunch energy differences for multiple-energy extraction with a one-third frequency subharmonic cavity.

As shown below, it will be desirable to have δW_{max} as small as possible. Therefore, a thin electrostatic septum will be used for the initial separation of the extracted pulses. This septum deflector will be placed near the center of the desired dispersive straight section orbit, where the dispersion function η is near its maximum. The pulses to be extracted will be further deflected by a septum magnet located at the downstream end of the straight section. The field requirements for this septum magnet to deflect the beam into a final extraction deflection magnet in the next linac straight section are modest (<0.8 kG). δW_{max} is determined by the condition

$$\eta(E)\delta W_{max}/E = \text{beam size} + \text{septum thickness}, \tag{10}$$

where E is the extracted beam energy and $\eta(E)$ is the dispersion function at the electrostatic septum. The beam size is determined by the horizontal and longitudinal emittance, both of which increase with E due to synchrotron radiation. The ratio $\eta(E)/E$ also decreases slowly with E. Therefore δW_{max} increases with the desired extraction energy. A δW_{max} sufficiently large to extract the intermediate-energy beam will be more than adequate for extraction of the low-energy beam.

The maximum intermediate-energy beam that can be extracted is actually limited by the low energy quadrupole apertures. If δW_{max} is the energy displacement required for extraction at some intermediate energy E, then the horizontal position of the energy-displaced pulses in one of the low-energy (E_1) dispersion sections quadrupoles can be as large as

$$\Delta X = \eta(E_1)\,\delta W_{max}/E_1, \tag{11}$$

Because of the nature of the focusing solutions in the low-energy dispersion regions, the dispersion function in some of the quadrupoles is much larger than the values at the ends of the straight sections. The ratio of $\eta(E_1)/E_1$ to the corresponding value at the electrostatic septum rises steadily to about 10 for the highest extraction energies.

The requirements are illustrated in Fig. 14. The left-hand scale shows δW_{max}. The three curves show the contributions from energy spread, horizontal emittance, and septum thickness. The right-hand scale shows the corresponding low-energy quadrupole half-aperture requirements. It has been assumed that the injected beam has horizontal and longitudinal 90% emittances of 0.05 mm-mrad and 30 keV deg. respectively. These emittances grow with energy due to synchrotron radiation as described in Section 7. The septum thickness S (which includes orbit errors) has been assumed to be 0.6 mm. Figure 14 shows that, based on the assumptions, if the apertures of the low-energy quadrupoles are limited to ± 2 cm, the intermediate extraction energy must be ≤ 3.1 GeV. The corresponding limiting value of δW_{max} is 1.3 MeV. The electrostatic field requirement for a 1 m deflector is less than 55 keV/m.

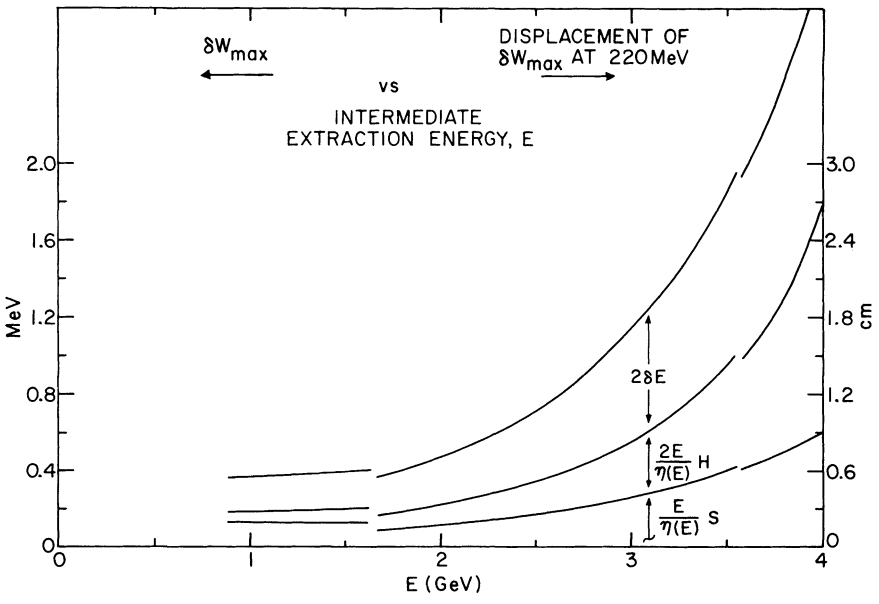

FIGURE 14 Maximum energy displacement δW_{max} (and corresponding horizontal displacement at 220 MeV) required for extraction of beam at energy E

$2\delta E$—dispersion in the beam

$2H$—width of horizontal betatron oscillation

S—septum thickness plus orbit error (0.6 mm total).

6. DIAGNOSTICS AND ORBIT CORRECTION SYSTEM

Commissioning and operation of the Hexatron would require sequential tuning of the beam in each dispersive straight section to optimize the beam position x_i, y_i, the synchrotron phase ϕ_s, the position of the waists of the beam and the value and slope of the dispersion η and η' through the following linac. Electron bunches must be directed down the axis of each linac with zero dispersion. The beams can be sequentially tuned from the lowest energy, starting with the beam from the injector. In order to understand diagnostic and control problems, it is necessary to determine how the required orbit parameters can be set on the basis of experimental measurements. We present a brief scenario of this procedure. Tune-up would be, of course, an iterative procedure.

Individual orbits on each turn would be initially adjusted to enter the linacs through the use of small bending magnets on each individual orbit in the dispersive straight sections. The measurement of the beam position of individual orbits in the linac section would be made either by sending a short bunch beam or a short notched beam through the microtron and using a low-Q cavity position detector of the sort used by the MAMI Microtron at Mainz.[24] Once the beam on an individual orbit is guided into the linac, it can be centered more precisely by means of a computer-control routine that would maintain minimum offset of the beam in both position and slope even in the presence of relatively large field and alignment errors. A three-point measurement of each individual orbit made at the entrance, center, and exit of the linac sections would be used. The beam manipulation and correction can be done in individual orbits in the dispersion sections by means of small correction-dipole elements.

Computer simulation of the control technique has been carried out for correction of horizontal and vertical orbit errors. The computer generated random errors in the sector bending magnets of $|\Delta B/B| \leq 0.00025$, alignment position Δx of $|\Delta x| \leq 0.0003$ m, and angular alignment ϵ of $|\epsilon| \leq 0.0004$ radians and in the quadrupoles of focal length f of $|\Delta f/f| \leq 0.001$, alignment position Δx of $|\Delta x| \leq 0.0003$ m, and alignment angle ϵ of $|\epsilon| \leq 0.0004$ m. The algorithms for generating the equilibrium-orbit errors have been previously described.[25] Typical results are shown in Fig. 15, where damped and undamped orbit displacements in the horizontal plane are

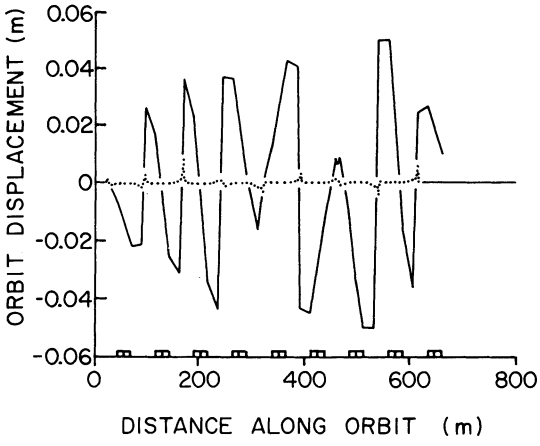

FIGURE 15 Results of computer simulation of horizontal damped (dotted line) and undamped (solid line) orbit displacements for 3 turns near 4 GeV.

compared for 3 turns near 4 GeV. Figure 15 shows the computer calculation of displacements in the equilibrium orbit for no correction (solid line) and after the computer control procedure is followed (dashed curve). These simulations indicate that residual orbit errors in the linac sections can be reduced to measurement error.

The overall tune of the machine can be verified quite accurately both for partial orbits or for many turns by pinging the beam with a small perpendicular kick at a variety of points in the linacs and watching subsequent perpendicular displacements. The distance between nodes of the displaced beam should accurately determine a betatron phase advance of $\Delta\phi = n\pi$, and this information would be used to trim quadrupoles. The dispersion of the beam through the linacs can be measured directly by comparing the horizontal position to the bunch energy variation $\eta = \Delta x/(\Delta E/E)$. Fluctuations in beam energy can be artificially introduced for this purpose at injection. The diagnostic pickups required for these measurements could be standard stripline or slot-couplers for high-frequency position measurements and resonant cavities for low-frequency measurements. It is possible to determine the positions of individual orbits in linacs in the presence of 36 other beams by the notch or pulse technique, as already discussed.[24] In addition detectors can be built that pick out transverse beam position of individual bunches of individual orbits when three separate intensities are being directed at three external targets by modulating the injected beam and tuning the slot or stripline detectors to be sensitive to particular modes of modulation.

The possibility that beam power might damage the accelerator is one that is common to other high-power accelerator facilities. Diagnostic safeguards against sudden damaging incidents are well tested at existing accelerators. Fast beam shutdown triggered by observation of increased beam loss in the accelerator can be accomplished by switching off the beam from the injector. Since the stored energy in the Hexatron beam is negligible (~ 10 J), all that is required is rapid response at the injector, although additional kickers could remove the beam from the ring in less than 1 μsec. Such procedures are standard at accelerators such as the 800 MeV linac LAMPF and the 20 GeV electron linac at SLAC.

7. EXPECTED OPERATING CHARACTERISTICS

The properties of the beams in the Hexatron will differ in several respects from those of synchrotrons and linear accelerators. Because the accelerating cycle to full energy is rapid in a microtron, no equilibrium is established between emittance growth and radiation damping. Consequently, in the Hexatron, particularly at higher energies, the transverse and longitudinal emittance will be determined by fluctuations in the synchrotron radiation. In addition, the maximum beam intensity will be limited by the onset of regenerative beam breakup, a phenomenon peculiar to recirculating accelerators. Because of the importance of these effects on the accelerator performance, we present a brief description of the salient points in this section.

A. Effects of Synchrotron Radiation

For the design parameters of Table I, the average energy loss per turn due to synchrotron radiation is 26.9 E^3 keV. At 4 GeV, this loss is 1722 keV. The growth rate per unit angle of deflection in the sector magnets of the horizontal average emittance

$\langle\epsilon\rangle$ due to fluctuations in this radiation is given by[26]

$$\frac{d\langle\epsilon\rangle}{d\theta} = H(s)\frac{\langle\Delta E^2\rangle}{E^2} \tag{12}$$

$$H(s) = \beta(s)\eta'^2(s) + 2\alpha(s)\eta'(s)\eta(s) + \gamma(s)\eta^2(s),$$

where $\langle\Delta E^2\rangle = \langle\delta E^2 - \langle\delta E\rangle^2\rangle$, δE is the energy loss per unit angle for an electron, the brackets denote an average over all electrons, β, α, γ are the horizontal Courant-Snyder parameters and η, η' are the dispersion-function components. Using a Poisson probability function for the photon emission gives $\langle\Delta E^2\rangle = \langle n\rangle\langle u^2\rangle$, where n is the average number of photons emitted per electron per unit bend angle and $\langle u^2\rangle$ is their mean square energy. Using the energy and field dependences of these terms given in Ref. 26, one can show that

$$\frac{\langle\Delta E^2\rangle}{E^2} = 43.1 \times 10^{-12}\frac{E^5}{r^2} = 3.99 \times 10^{-12}E^3 \tag{13}$$

in the Hexatron for a magnetic field of $1T$, where E is in GeV.

Substituting the known functional behavior of the Courant-Snyder parameters for 4 GeV operation (for a more detailed account, see Ref. 27) into H in Eq. (12) gives for growth rate per 1/3 turn the result

$$\Delta\langle\epsilon\rangle(1/3\text{ turn}) = (0.3171E^5 + 6.598E^4 + 79.025E^3 - 1.79E^2)10^{-6}\text{ mm-mrad}, \tag{14}$$

where E is in GeV.

Acceleration in the linac sections provides some damping, but quadrupole and other error fields will lead to a growth of the normalized emittance. If one assumes a factor of 5 for the normalized emittance growth due to these other causes the energy dependence of the high energy emittance will be

$$\langle\epsilon\rangle(4\text{ GeV}_{\max}) = 10^{-6}[1.399E^6 + 34.398E^5 + 503.7E^4 - 25.5E^3]\text{ mm-mrad} \tag{15}$$

independent of the initial conditions. [Eq. (15) is valid for 4 GeV operation since it assumes a 1 T field and 35 MeV energy gain per linac.] The value predicted for $\langle\epsilon\rangle$ at 4 GeV is 0.17 mm-mrad. The amount of non-radiative growth assumed for the normalized emittance has very little effect on the final emittance. If one assumes complete linac damping, the final result is 0.15 mm-mrad. No effective linac damping gives a final result of 0.19 mm-mrad.

The synchrotron-radiation fluctuations that cause the phase-space growth are a random process. Therefore one expects the density function along either axis of the two dimensional phase space to be Gaussian. Computer simulation (described below) of beam growth verifies this assumption. Therefore the density function for ϵ is exponential and $\pi\langle\epsilon\rangle$ is the phase-space area that contains 63% of the beam. Ninety percent and 99% of the beam are contained within the emittance values of $\epsilon = 2.3\langle\epsilon\rangle$ and $\epsilon = 4.6\langle\epsilon\rangle$, respectively. The mean-square half-width of the beam at any location

having the Courant-Synder parameter β is

$$\sigma_x^2 = \frac{\beta\langle\epsilon\rangle}{2} \tag{16}$$

At the ends of the linacs, where $\beta = 25.4$, the emittance values predicted by Eq. (15) show that 99% of the electrons should have oscillation amplitudes less than 4.5 mm at 4 GeV.

The growth of the average longitudinal emittance $\langle\epsilon_s\rangle$ per 1/3 turn may be written as

$$\Delta\langle\epsilon_s\rangle(1/3 \text{ turn}) = 2\int_0^{\pi/3} \beta_s\langle\Delta E^2\rangle\, d\theta, \tag{17}$$

where β_s is the longitudinal Courant-Synder parameter at the angle θ in a sector magnet. Actual integration of Eq. (17) for parameters corresponding to a synchronous phase of 18° gives

$$\Delta\langle\epsilon\rangle(\text{per } 1/3 \text{ turn}) = \frac{16.43}{W}\langle\Delta E^2\rangle. \tag{18}$$

Since the energy gain per linac is $\Delta W/3$, one has

$$\langle\epsilon_s\rangle = \langle\epsilon_s\rangle_0 + \int_{E0}^{E} \frac{49.29}{(\Delta W)^2}\langle\Delta E^2\rangle\, dE = \langle\epsilon_s\rangle_0 + 0.17\,(E^6 - E_0{}^6)\text{ keV deg}, \tag{19}$$

where E and E_0 are in GeV. This gives $\langle\epsilon_s\rangle = 700$ keV deg at 4 GeV. Since $\langle\Delta E^2\rangle$ and W^2 in Eq. (16) are both proportional to $E_{\max}^2$, Eq. (16) is the correct expression for any value of $E_{\max}$.

To provide further confirmation of these results, the effects of fluctuations in synchrotron radiation on the behavior of the electrons in four-dimensional phase space have been studied by computer simulation. Because the final phase-space volume is large compared with the initial volume, the final density function is almost independent of the initial choice of phase-space points. Typically, the choice has been an initial volume that has 90% projected areas of 0.05π mm-mrad and 30π keV deg in the transverse and longitudinal phase space. The program computes the motion of the phase points as they lose energy by random processes in the sector magnets and are accelerated to the final orbit by the linacs.

The results show the expected behavior of the phase-space center. The individual phase points move around the center with amplitude growth rates that agree with the predicted results. The ratios of the first four moments agree, to within statistical fluctuations, with the ratios expected for exponential area distributions. This fact gives confidence in the assumption that the phase-space areas containing up to 99% of the particles can be estimated from the theoretical expression for $\langle\epsilon\rangle$ in the two planes. Figures 16 and 17 show the final phase points at the linac center for a typical run with 500 particles. The ratios of the vertical to the horizontal scales have been adjusted so that the constant density contours should be circles. The circles drawn on the figures are those that enclose the given fraction of the particles.

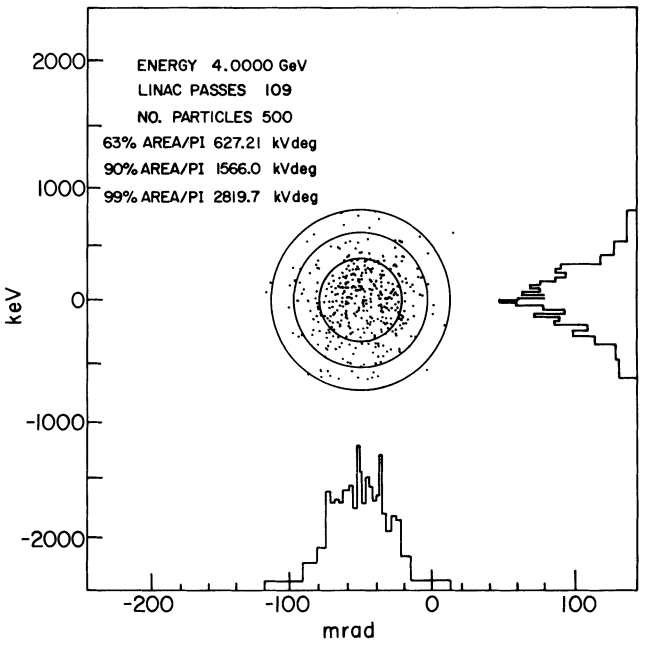

FIGURE 16 Longitudinal phase-space distribution of Hexatron beam at linac center at 4 GeV.

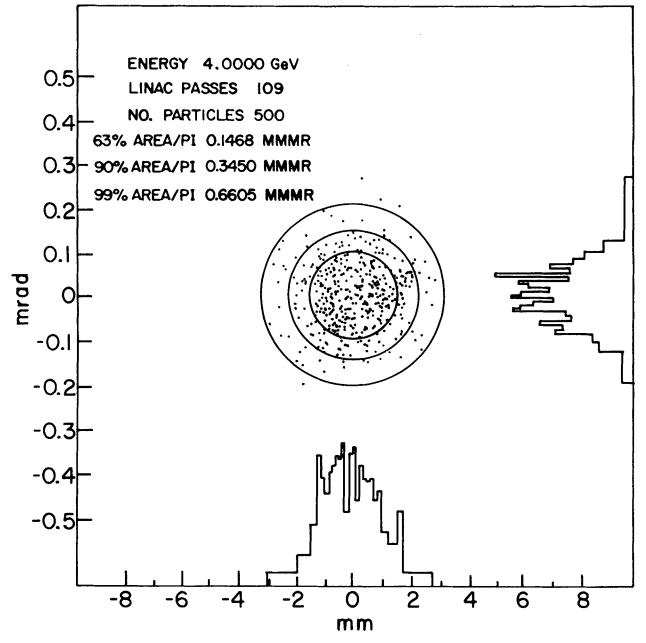

FIGURE 17 Horizontal phase-space distribution of Hexatron beam at linac center at 4 GeV, corrected for orbit distortion.

B. Closed-Orbit Distortions

To compensate for the synchrotron-radiation energy loss, the rf average phase error slips gradually to -50 mrad during acceleration. A computer program was used to follow the mean 4-dimensional phase-space motion of a particle that starts at the origin at injection, radiates energy in the sector magnets, and is accelerated in the linac sections. The results indicate that a quasi steady-state condition develops after the first few orbits where the energy errors upstream and downstream of the linacs are nearly equal and opposite. An increasing negative slope develops in the linac sections, producing positive and negative displacements in the two sector magnets.

The maximum angle at 4 GeV is 1 mrad, producing ± 1.2 mm of displacements at the two ends of the linac. The distortion in the linac sections can be completely eliminated by providing more bending moment in the linac downstream sector magnets where the energy error is positive and less in the linac upstream sector magnets where the energy error is negative. Thus, one needs to add equal and opposite small magnets at the two ends of the dispersion section. The dispersion straight sections should also be tilted so that the orbits pass along the optical axis. The optical axis displacements and bends required to make the orbits lie on the linac center lines are small and have values of ± 0.3 mm and ∓ 0.013 mrad at 4 GeV.

C. Regenerative Beam Breakup

The onset of regenerative beam breakup (RBBU) arises because cw beams can excite transverse deflecting modes in the linac sections. These modes produce forces on the injected beam that drive it out of the acceptance region of the accelerator on its first traversal of the linac when its magnetic rigidity is lowest. This type of breakup has been studied in some detail by Volodin and Hanson,[28] Herminghaus and Euteneur,[29] Vetter[30] and Rand.[31]

The mechanism for RBBU is complex and the recirculation optics play a crucial role. To develop a credible model for the process in a specific recirculator, one must know the properties of the transverse deflecting modes in the linac structures, their frequencies and Q's, the details of the orbit containment optics, and the exact geometries of the particle trajectories. The linac and beam optics in a special design must be optimized for maximum starting current. Rand[31] has developed an approximate formula which does not take account of the detailed features of the accelerator structure or of the beam optics of the accelerator, but which is useful for estimating the magnitude of starting current for regenerative breakup, and assessing its dependence on various parameters. The Rand "rule of thumb" for multi-sided microtrons is

$$I_s \approx \frac{M\gamma_i^*(1 + \gamma_0/\gamma_i)L_s n}{Q_L N^2 L_0 (n-1)^2}, \tag{20}$$

where M varies from 1 to 5×10^4 amps depending on the recirculation optics. The electron energy at injection is γ_i, γ_i^* is the electron energy at the center of the first isolated linac section, γ_0 is the energy gain per turn in units of m_0c^2, L_s is the linac section length, L_0 is the total linac length, and N is the number of cells per linac section. Finally n is the number of turns to extraction energy, and Q_L is the loaded Q of the HEM deflecting mode. It is evident from this formula that high injection energy,

minimum number of recirculations, and highest accelerating voltage gradient together with shortest possible linac allow the highest starting currents.

A more detailed treatment of this model of RBBU has been used[31] to estimate starting currents for a number of proposed recirculating accelerators. Estimates of the threshold for RBBU in the GEM design can be made by extrapolating these data with the aid of Eq. (20). While such an extrapolation is, of necessity, crude, the results suggest that the proposed design will operate comfortably below the expected RBBU threshold. If Eq. (20) is used as a figure of merit, the GEM Hexatron is close to the ANL 2 GeV DSM design discussed in Ref. 31. The "worst-case" predicted threshold for RBBU in this case is ≈ 740 μA, well above the 300 μA expected maximum current for GEM. The essential differences in the GEM design are shorter linac sections, a larger energy gain per turn, and a longer total linac length. Each of these differences favors an increased threshold for RBBU.

Attempts to observe RBBU in room-temperature recirculators thus far have failed. A 14 MeV 20-turn racetrack microtron has operated routinely[32] with cw beams of up to 90 μA. Attempts to test breakup calculations have been made[33] by looking for amplification of transverse beam noise imposed by means of an rf cavity on the injection path. The beam noise, at $\nu = 4175 - 4205$ MHz was detected by a similar cavity at the output of the RTM. No evidence of a resonance of beam noise was observed, although the region near 4200 MHz is expected to be particularly troublesome. In summary, the limited evidence available suggests that there is not a fundamental limit imposed on the design presented here at the operating levels proposed.

8. HIGH-ENERGY OPTIONS

Although the maximum energy of the design presented here is 4 GeV, recent developments make it clear that with no substantial engineering modification, the present configuration could be operated in a cw mode at maximum energies between 4.5 and 5 GeV. The high-energy limit in a Hexatron configuration is determined by four factors: rf voltage gradients attainable in the linacs, field saturation and error fields in the sector magnets associated with operation above 1 T, and the beam-emittance growth induced by synchrotron radiation. The limit on the rf accelerating gradient is set by the power that can be absorbed by the waveguides themselves. Recent tests on the side-coupled wave guides cited in Section 4d have shown that 48.5 kW/m could be dissipated without significant detuning of the structures. With shunt impedance of 67–68 $M\Omega$/m predicted for a linac with a 1.6-cm bore, the corresponding maximum beam energy would be 4.46 GeV for Hexatron linacs with 11 sections, as discussed. The use of an additional 3 m of linac, running at full power, could be added raising the final beam energy to 4.8 GeV in full cw operation. Operation at 4.5–5 GeV would require corresponding increases in the Hexatron sector-magnet fields. The sector magnets could be operated with additional ampere turns to provide the increased flux density, or additional iron could be added to the yokes. Such an increase in the dynamic range of the Hexatron would dictate the use of the system of transverse beam optics that does not require steps in the sector magnets (see Section 4b). This choice would minimize contributions of error fields due to saturation effects.

The ultimate limit on the operating point is determined by the emittance growth due to synchrotron radiation. Calculations similar to those of Section 7a modified for the higher energy gain per turn indicated that at 5 GeV the beam area corresponding to

99% of the change would fill the linac bore at the entrance and exit and at 6 GeV the area corresponding to 90% of the beam would fill the bore. For operation above 4 GeV, it would be necessary to protect the linacs with collimators and scrapers placed at the linac entrances. For operation above 5 GeV, it would be necessary to operate the Hexatron in a long pulse mode corresponding to a duty factor near 60% and at beam currents limited by power dissipation on the collimators.

9. CONCLUDING REMARKS

The microtron configuration offers a very powerful option for generating intense cw electron beams for energies up to about 5 GeV. For energies below 1 GeV, conventional racetrack design are already establishing new levels of performance.[4] For operation above 1 GeV, the multi-sided microtron variants, so-called polytrons, show great promise. The 4 GeV Hexatron design presented here has the advantages of excellent beam quality, modest power requirements, and capability of furnishing beams of several energies and intensities simultaneously. It is perhaps the ideal choice for the acceleration of polarized electrons in this energy range for several reasons. First, in contrast to cyclical accelerators, e.g. storage and stretcher rings, most resonant depolarizing effects are absent in the Hexatron. Second, in contrast to alternative options, the polarized electron source in the Hexatron operates in a truly cw mode with low instantaneous currents. This feature opens new possibilities[34] for increasing the stability and maximum polarization of polarized electron beams.

Finally, the principal shortcoming of the Hexatron design that limits its performance at higher energy is the onset of emittance growth induced by synchrotron-radiation fluctuations. Even here there are design options to be explored that may ameliorate this effect. For example, if radial focusing were introduced in the sector magnets to limit the maximum values of the radial beta function the growth would be considerably suppressed. The multi-sided microtron is a relatively new concept and such options remain to be explored.

ACKNOWLEDGMENTS

It is a pleasure to acknowledge the valuable discussions and insights of Dr. Karl-Heinz Kaiser, who served as a consultant to the GEM Project. In addition, the authors wish to express their gratitude to W. E. Massey, Laboratory Directory and K. L. Kliewer, Associate Laboratory Director, for their warm support and continuing interest through all the tribulations of the GEM design effort.

REFERENCES

1. V. I. Veksler, *Proc. USSR Acad. Sci.*, **43,** 346 (1944).
2. K.-H. Kaiser, "A Possible Magnet Field Configuration for a CW Electron Accelerator in the GeV Region", in *Proceedings of the Conference on Future Possibilities for Electron Accelerators*, J. S. McCarthy and R. R. Whitney, editors, page V, (January 1979).
3. "Conceptual Design of a 4-GeV Hexagonal Microtron", T. K. Khoe, contributed Paper, *Proceedings of Conference on New Horizons in Electromagnetic Physics*, Charlottesville, April 21–24, 1982, J. V. Noble and R. R. Whitney, editors, University of Virginia.
4. K.-H. Kaiser, *Bull. Amer. Phys. Soc.*, **28,** 978 (1983).
5. S. Penner, *et al.*, *IEEE Trans. Nucl. Sci.*, **NS-28,** 1526 (1981).

6. H. E. Jackson, editor, Argonne National Laboratory Report ANL-82-83, "A National CW GeV Electron Microtron Laboratory" (1983).
7. E. Herminghaus, *et al.*, *Nuclear Instruments and Methods*, 138 (1976).
8. H. S. Kreidel and K. Merle, "Automatic Beam-Steering of the Mainz Microtron", *Proceedings of the 1981 Linac Conference*, Sante Fe, New Mexico, 1981.
9. P. Debenham, *IEEE Trans. Nucl. Sci.*, **NS-28,** 2885 (1981).
10. H. A. Enge, *Rev. Sci. Instrum.*, **35,** 278 (1964).
11. A. M. Winslow, *J. Comput. Phys.* **2,** 149 (1967).
12. R. B. Wehrle *et al.*, "Prototype Sector Magnets for the GeV Electron Microtron (GEM)", *IEEE Trans. Nucl. Sci.*, **NS-30,** 2859 (1983).
13. J. Simpkin and C. W. Trowbridge, "Three Dimensional Non-Linear Electromagnetic Field Computation using Scalar Potentials", *IEEE Proceedings*, **127,** Part B, # 6 (1980); J. Simpkin, TOSCA User Guide 3D Static Electromagnetic/Electrostatic Analysis Package. Version 3.1, May 1982, RL-81-070.
14. K. M. Thompson, R. J. Lari, and R. B. Wehrle, J. Phys., to be published.
15. J. Gervaise, "High Precision Instrumentation developed for CERN", CERN Report CERN SPS SA/81-1.
16. P. F. Pellisier, *IEEE Trans. Nucl. Sci.*, **NS-12,** 19 (1965).
17. E. A. Knapp, B. C. Knapp, and J. M. Potter, *Rev. Sci. Instrum.*, **39,** 979 (1968).
18. S. O. Scriber, E. A. Heighway, and L. W. Funk, *Proc. of 1972 Proton Linac Conf.*, LANL Report No. LA-5115, 114 (1972).
19. V. G. Andreev, V. M. Belugin, V. G. Kulman, E. A. Mirochnik, and B. M. Pirozenko, "Study of High-energy Proton Linac Structures", in *Proceedings of the 1972 Proton Linear Accelerator Conference*, LANL Report LA-5115, 114.
20. Y. Iwashita, *IEEE Trans. Nucl. Sci.*, **NS-30,** 3542 (1983).
21. S. R. Scriber, "Room Temperature Cavities for Accelerating Structures", in *Proceedings of the Conference on Future Possibilities for Electron Accelerators*, J. S. McCarthy and R. R. Whitney, editors, page K (January 1979).
22. Lyold Young, Los Alamos National Laboratory, private communication.
23. S. O. Scriber *et al.*, *Proc. of the 1976 Proton Linear Accelerator Conf.*, Chalk River, AECL-5677, pp. 338, 405.
24. H. Herminghaus, B. Dreher, H. Futeneur, K. H. Kaiser, M. Kelliher, R. Klein, H. J. Kreidel, M. Loch, U. Ludwig-Merlin, K. Merle, H. Schoeler, R. Schulze, P. Semmel, and G. Stephen, *IEEE Trans. Nucl. Sci.*, **NS-30,** 3274 (1983).
25. R. L. Kustom, *IEEE Trans. Nucl. Sci.*, **NS-30,** 3229 (1983).
26. Matthew Sands, "The Physics of Electron Storage Rings", SLAC 121, (1970).
27. E. A. Crosbie, *IEEE Trans. Nucl. Sci.*, **NS-30,** 3218 (1983).
28. V. A. Volodin and A. O. Hanson, *IEEE Trans. Nucl. Sci.*, **NS-22,** 1194 (1975).
29. H. Herminghaus and H. Euteneur, *Nucl. Instrum. Methods*, **163,** 299 (1979).
30. A. M. Vetter, HEPL Report 869 (1980).
31. C. M. Lyneis, R. E. Rand, H. A. Schwettman, and A. M. Vetter, *Nucl. Instrum. Methods*, **204,** 269 (1983).
32. H. Aufhaus, *et al.*, *Proceedings of the 1981 Linear Accelerator Conference*, LANL Report LA 9234-C, 22.
33. H. Euteneur, H. Herminghaus, and R. Klein, *Proceedings of the 1981 Linear Accelerator Conference*, LANL Report LA-9234-C, "Instabilities in Race Tract Microtrons", p. 239.
34. P. A. Sander, V. W. Hughes, M. S. Lubell, and S. Kowalski, in *Future Directions* in "Electromagnetic Nuclear Physics," P. Stoler, Rensselaer Polytechnic Institute, editor, p. 385 (1981).